Solar Phys (2013) 288:89–103
DOI 10.1007/s11207-013-0313-9

Doppler Shifts of the Hα Line and the Ca II 854.2 nm Line in a Quiet Region of the Sun Observed with the FISS/NST

Jongchul Chae · Hyung-Min Park · Kwangsu Ahn · Heesu Yang · Young-Deuk Park · Kyung-Suk Cho · Wenda Cao

Received: 13 August 2012 / Accepted: 24 April 2013 / Published online: 5 June 2013

Abstract The characteristics of Doppler shifts in a quiet region of the Sun are compared between the Hα line and the Ca II infrared line at 854.2 nm. A small area of $16'' \times 40''$ was observed for about half an hour with the Fast Imaging Solar Spectrograph (FISS) of the 1.6 meter New Solar Telescope (NST) at Big Bear Solar Observatory. The observed area contains a network region and an internetwork region, and identified in the network region are fibrils and bright points. We infer Doppler velocity v_{m} from each line profile at each individual point with the lambdameter method as a function of half wavelength separation $\Delta\lambda$. It is confirmed that the bisector of the spatially averaged Ca II line profile has an inverse C-shape with a significant peak redshift of $+1.8$ km s^{-1}. In contrast, the bisector of the spatially averaged Hα line profile has a C-shape with a small peak blueshift of -0.5 km s^{-1}. In both lines, the bisectors of bright network points are significantly redshifted not only at the line centers, but also at the wings. The Ca II Doppler shifts are found to be correlated with the Hα ones with the strongest correlation occurring in the internetwork region. Moreover, we find that here the Doppler shifts in the two lines are essentially in phase. We discuss the physical implications of our results in view of the formation of the Hα line and Ca II 854.2 nm line in the quiet region chromosphere.

Keywords Chromosphere, quiet · Spectral line, intensity and diagnostics

Initial Results from FISS
Guest Editor: Jongchul Chae

J. Chae (✉) · H.-M. Park · H. Yang
Astronomy Program, Department of Physics and Astronomy, Seoul National University, Seoul 151-747, Korea
e-mail: chae@astro.snu.ac.kr

Y.-D. Park · K.-S. Cho
Korea Astronomy and Space Science Institute, Daejeon, Korea

K. Ahn · W. Cao
Big Bear Solar Observatory, New Jersey Institute of Technology, 40386 North Shore Lane, Big Bear City, CA 92314, USA

1. Introduction

The chromosphere – traditionally referring to the layer seen outside the solar limb that emits intense light in the Hα line and other very strong lines in the visible and near-infrared spectra – still remains mysterious in many aspects (Rutten, 2010). This layer, particularly its outer part, comprises a number of inhomogeneous plasma features relevant to flows, waves, shocks and magnetic fields.

The simultaneous recording of the Hα line and one of the Ca II lines is a useful diagnostic of these features, particularly if their Doppler absorption widths can be measured. Because of the big difference in atomic mass, the absorption width of the Hα line is dominated by thermal broadening, and that of the Ca II line, by non-thermal broadening, which allows us to separately determine temperature and the speed of non-thermal motion. This kind of atomic weight tool was previously exploited by Scoas-Navarro and Elmore (2005) with the Ca II infrared lines and the He I line at 1083 nm, and by Cauzzi *et al.* (2009) with the Hα line and Ca II 854.2 nm line.

It is quite worthwhile to investigate the characteristics of Doppler shift in the chromosphere by comparing between the Hα line and the Ca II line. We expect that the Doppler shifts in the two lines would be the same or at least be correlated with each other, if the two lines are absorbed by the same volume in the chromosphere, a prerequisite for the atomic weight tool above to be applicable. As a matter of fact, comparing Doppler shifts between different chromospheric lines is not new in solar physics (*e.g.* Cram, Brown, and Beckers, 1977), but is recently becoming important again with the arrival of new instruments like IBIS (*e.g.* Cauzzi *et al.*, 2009) or CRISP (*e.g.* Sekse, Rouppe van der Voort, and De Pontieu, 2012).

Different methods have been used to infer Doppler shifts from the chromospheric lines. The early measurements were done with the Dopplergram technique that compares intensity between two wavelengths $\pm\,\Delta\lambda$ offset from the center of the reference line as in the case of weaker lines of photospheric origin (Leighton, Noyes, and Simon, 1962). Since the full line profile became available, the wavelength of minimum intensity or line center has frequently been used as a measure of Doppler shift (Cram, Brown, and Beckers, 1977; Lites, Rutten, and Kalkofen, 1993; Cauzzi *et al.*, 2008). More general, but less widely used is the so-called lambdameter method (Deubner, 1974; Mein and Mein, 1976; Deubner, Waldschik, and Steffens, 1996). For given length $2\Delta\lambda$, this method seeks the wavelength of the middle point of a horizonal chord of the given length that fits into the line profile. It usually uses the inner wings to infer Doppler shift instead of the line center. This method yields the intensity of the chord as well, and the series of such wavelength-intensity pairs obtained for different values of $\Delta\lambda$ naturally leads to the construction of the bisector of the line profile.

The bisector of a line profile provides much information on the velocity field and the formation of the line. It has been well known that the bisector of a strong photospheric line is usually shaped like a distorted C, which is successfully explained by the combined effect of hot rising material and cool falling material in the granulation together with the fact that the core of a strong line is formed high in the photosphere above the granulation (Gray, 1992; Asplund *et al.*, 2000). The bisectors of chromospheric lines, however, are not well established observationally, and even little understood. It is only several years ago that Uitenbroek (2006) first reported an interesting finding that "spatially averaged intensity profiles of the chromospheric Na I D and Ca II infrared lines exhibit a pronounced red asymmetry in their cores with bisectors in the shape of an inverse C." This finding is contrasted with the well-known C-shape in the bisectors of spectral lines of photospheric origin.

In this paper we investigate the observed characteristics of Doppler shifts of the Hα line and Ca II 854.2 nm line in different kinds of features in a quiet region of the Sun. Using the

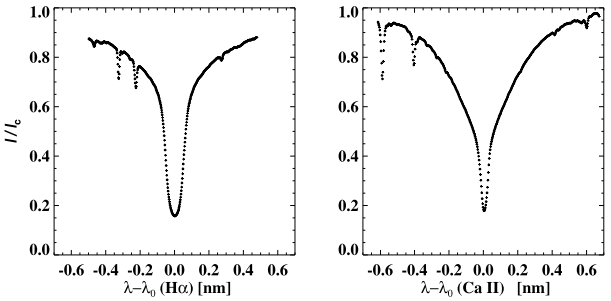

Figure 1 Quiet Sun profiles of the Hα (left) and Ca II 854.2 nm lines (right) obtained by averaging over $16'' \times 40''$ and over about half an hour. Telluric lines in the line cores were removed.

Fast Imaging Solar Spectrograph (FISS) of the 1.6 meter New Solar Telescope (NST) at Big Bear Solar Observatory, we observed a quiet region near the center of the solar disk for about half an hour. The FISS is a dual band Echélle spectrograph that can record high-resolution spectra of the Hα line and the Ca II 854.2 nm on two different cameras simultaneously (Chae *et al.*, 2012).

We study observational properties of Doppler shifts that may serve as a basis for our future goal of determining the physical parameters of different kinds of features from the observed line profiles. The categories of the features we deal with are

i) all the features in the whole quiet region,
ii) all the features in the internetwork region,
iii) Hα fibrils and Ca II fibrils in the network region, and
iv) bright points in the network region.

For each group of the features, we examine characteristics of average Doppler shifts from the bisectors of spatially averaged spectral profile of each line, and the characteristics of their spatio-temporal fluctuations based on the RMS values and cross-correlations of Doppler shifts.

2. Observation and Analysis

2.1. Observation

The FISS is an imaging spectrograph that successively takes a pair of spectrograms at the dual bands at each location of the slit inside the field of view. With this instrument we observed a small quiet region of $16'' \times 40''$ on 13 July 2011. Each Hα line spectrogram comprises 512×256 pixels of 1.9 pm (picometer) $\times\, 0.16''$, covering 0.97 nm (nanometer) $\times$ $40''$, and each Ca II 854.2 nm line spectrogram, 502×250 pixels of 2.6 pm $\times\, 0.16''$, covering 1.3 nm $\times\, 40''$. Figure 1 presents the profiles of the two lines averaged over the observed quiet region.These are representative of the quiet Sun in that they are averaged over a disk-center area that includes both network and internetwork, and over a time span that is much longer than the predominant periods of solar oscillations.

The FISS does imaging based on the fast scan of the slit over the field of view. The step size was set to $0.16''$, and each scan of 100 steps was done in 18 s. The scan was repeated for about half an hour. The resulting field of view of the observed region is $16'' \times 40''$ or 12 Mm $\times$ 29 Mm. Figure 2 shows the raster images constructed from a set of one scan data at the fixed wavelengths. The figure shows that even though small, the field of view is still big enough to contain typical network features as well as internetwork features. The

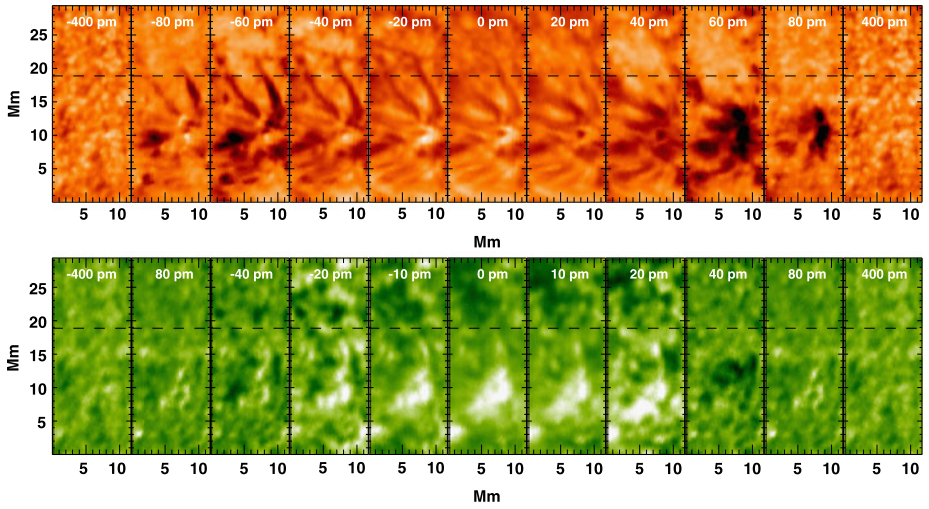

Figure 2 Images of the observed region constructed from one raster scan at different wavelengths of the Hα line (upper) and the Ca II 854.2 nm line (lower). The horizontal dashed lines indicate the boundary between the network region and the internetwork region.

early run performance of the FISS as well as basic data processing was described by Chae *et al.* (2012). The basic processing of data includes dark subtraction, flat fielding, distortion correction, and noise suppression.

The spatial resolution of the Hα data in this observation is estimated to be better than 1″, and that of the Ca II 854.2 nm data, to be poorer, as was reported by Chae *et al.* (2012). These resolutions fall short of the diffraction-limited resolutions of the NST – 0.10″ and 0.13″ – mainly for two reasons. First, the troublesome seeing is to be corrected by the adaptive optics (AO) only with post image processing being impossible, but the currently operating AO is not optimized for visible wavelengths and quiet region observations. In addition, we realize that the relay optics of the FISS in early observations that produced the current data was not optimal, being subject to ill-focusing and chromatic abberation. Upon the improvement of both the AO and the relay optics, future FISS observations will have much higher spatial resolution, even though not as high as diffraction-limited ones.

2.2. Wavelength Calibration

We have calibrated wavelengths by setting the rest frame to the center of the Sun. The adopted laboratory wavelengths of the Hα line and the Ca II line are 656.2817 nm and 854.2089 nm, respectively. In each of the Hα band and Ca II 854.2 nm band, this wavelength calibration is done in two steps. First, wavelength is calibrated in the rest frame of the Earth using two telluric lines in each band – the H_2O lines at 656.1097 nm and 656.4206 nm in the Hα band, and the H_2O lines at 854.0817 nm and 854.6222 nm in the Ca II band. Next, the radial velocity of the Sun relative to the Earth is calculated based on the ephemeris data of the Sun, and the corresponding Doppler shift is subtracted from the above wavelength values, resulting in the wavelengths calibrated in the rest frame tied to the center of the Sun. Our wavelength calibration is distinct from the conventional approach defining the zero of Doppler shift as the spatial average over the whole data set (Deubner and Fleck, 1990; Cauzzi *et al.*, 2008).

2.3. Removal of Telluric Lines

After wavelength calibration, we removed telluric lines near the line cores in the following steps. First, we identify the center of each telluric line, and define two small spectral regions surrounding the line. Second, the intensity variation in the two spectral regions is fitted by a regularly varying low-order polynomial function. Finally, the intensity variation in the local spectral region containing the telluric line is replaced by this function.

2.4. Lambdameter Method

With the observed spectral profile $I(\lambda)$ and half the length of the chord $\Delta\lambda$ given, the lambdameter method (Deubner, Waldschik, and Steffens, 1996) calculates the Doppler (line-of-sight) velocity $v_{\rm m}$ from the middle wavelength of the chord, $\lambda_{\rm m}$ that satisfies $I(\lambda_{\rm m} - \Delta\lambda) = I(\lambda_{\rm m} + \Delta\lambda) = I_1$ where the intensity of the chord I_1 is obtained as a byproduct. In this lambdameter method both I_1 and $\lambda_{\rm m}$ are considered as functions of $\Delta\lambda$. The bisector of a spectral line is nothing but the plot of all the pairs of $I_1(\Delta\lambda)$ *vs.* $\lambda_{\rm m}(\Delta\lambda)$ obtained with different values of $\Delta\lambda$. Note that $I_1(\Delta\lambda)$ and $\lambda_{\rm m}(\Delta\lambda)$ are independent of each other.

3. Feature Identification

The comparison of Figures 2 and 3 shows that the two lines differ in prominently visible features. In the network region, fibrils are conspicuous in the Hα line, and bright network points, in the Ca II line. As is well known (*e.g.* Cauzzi *et al.*, 2009), the Hα line core intensity mostly reflects light-scattering features, while the Ca II line core intensity is sensitive to temperature. Specifically, Leenaarts, Carlsson, and Rouppe van der Voort (2012) found from their state-of-art modeling of the Hα line formation that the core intensity is correlated with the average formation height. The internetwork region (hereafter IN) contains roundish dark features seen either at Ca II + 20 pm or at − 20 pm, but not at both wavelengths. They hence represent the shift or distortion of the Ca II line profile due to the presence of material moving either upward or downward, for example, during the passage of shock waves (Vecchio, Cauzzi, and Reardon, 2009).

Can we identify bright network points in Hα and fibrils in Ca II in the network region? Leenaarts *et al.* (2006a) and Leenaarts *et al.* (2006b) showed that Hα blue wing images are the best proxy for photospheric magnetic features. Bright points, however, are not obvious in our Hα images, probably because overlying fibrils are blocking out bright network points below. Meanwhile, Cauzzi *et al.* (2008) discovered a number of fibrils in the Ca II line using high-resolution observations with IBIS. In our Ca II observations, however, fibrils are not clearly visible. This may be partly because the spatial resolution of our Ca II data is not high enough, and partly because the Ca II fibrils may be intrinsically short (Rouppe van der Voort *et al.*, 2009; Cauzzi *et al.*, 2009). Note that this network region is not an enhanced one hosting many stable long fibrils. Nevertheless, a careful look at Figures 2 and 3 near the Hα fibrils reveals a few fibril-like structures in our Ca II images particularly at the wavelengths of ± 20 pm. Like the Hα fibrils, these "Ca II fibrils" appear dark and somewhat elongated, and extend radially out from the bright points, even though not so clearly defined as the Hα fibrils are.

Our feature recognition was done in every set of images constructed from each raster scan, based on the ratio of $I_1(\Delta\lambda)$ to the mean value of the quiet region. The choice of $\Delta\lambda$

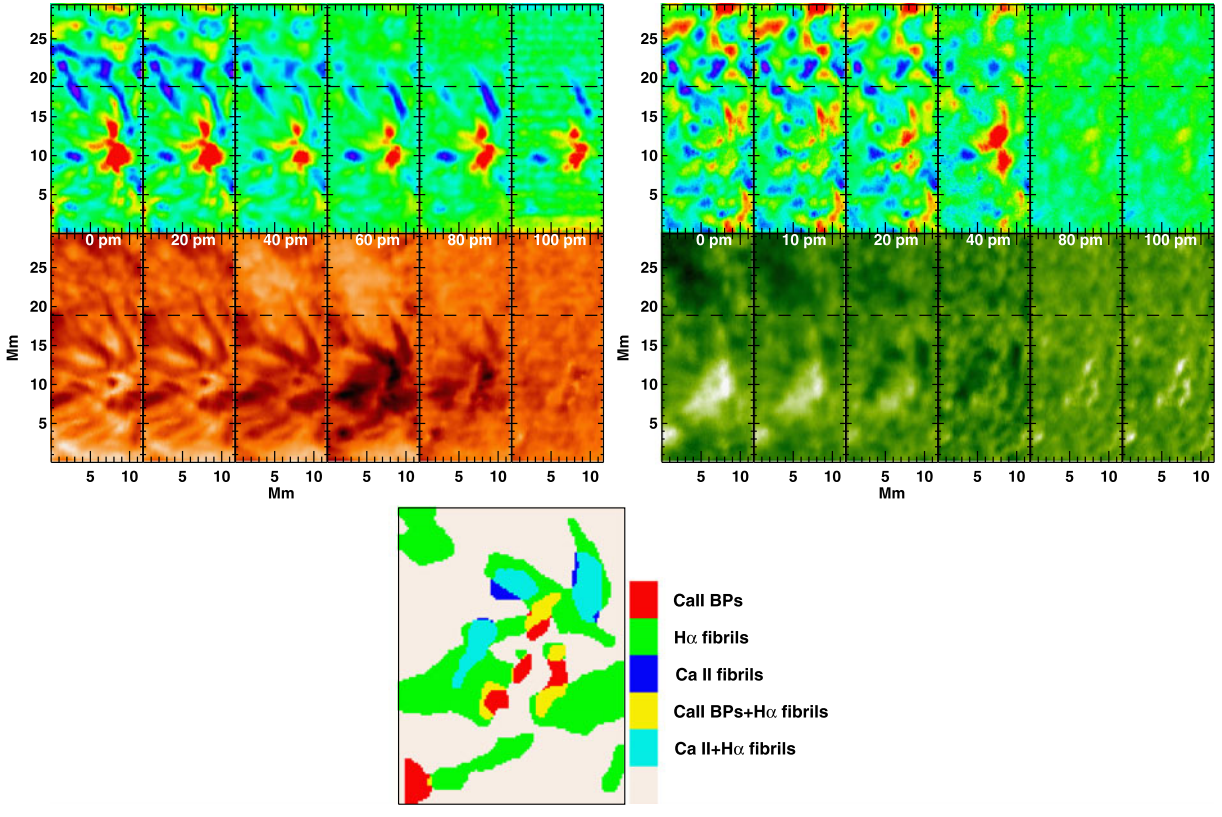

Figure 3 Top: Maps of $v_{\rm m}$ for different values of $\Delta\lambda$ from the Hα line (left) and the Ca II 854.2 nm line (right). For display the maps of $v_{\rm m}$ were scaled by $\pm 5\,{\rm km\,s^{-1}}$ (Hα) and $\pm 2.5\,{\rm km\,s^{-1}}$ (Ca II), respectively. Middle: Maps of I_1 constructed at the same wavelengths. Bottom: feature identification in the network region (below the horizontal line). Note that Ca II BPs identified here are well visible in the I_1 map of Ca II with $\Delta\lambda = 100$ pm, Hα fibrils, in the Hα map with $\Delta\lambda = 60$ pm, Ca II fibrils in the Ca II map with $\Delta\lambda = 20$ pm.

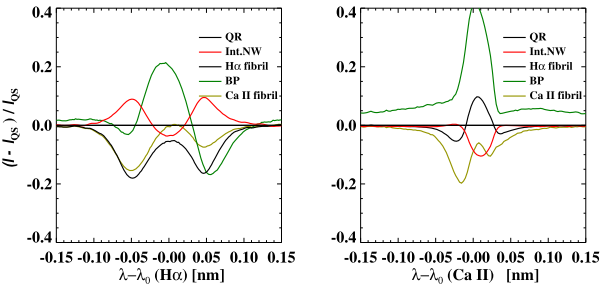

Figure 4 Mean contrast profiles of the Hα line and the Ca II 854.2 nm line for each kind of features.

and the threshold value depends on the feature. The bottom panel of Figure 3 illustrates our feature identification in the network region in a specific raster scan. The Hα fibrils occupy a significant portion of the region. The Ca II fibrils are shorter than the Hα fibrils, but a great part of these Ca II fibrils overlap the Hα fibrils, suggesting that the Ca II fibrils are not fully distinct from the Hα fibrils. The Ca II bright points partly overlap the Hα fibrils, even though they must be mutually different. The white areas refer to the unidentified regions inside the network region, and are excluded from our analysis below.

The mean contrast profiles in Figure 4 shows the spectral property of each kind of features. The left panel shows that the Hα fibrils, the most conspicuous features in Hα, appear as absorption features at all wavelengths in that they are darker than the quiet region average. The peak dark contrast of -0.17 occurs at wavelengths of about ± 50 pm. The Hα contrast profile of the Ca II fibrils is similar to the Hα fibrils, except that their dark contrast at $+50$ pm is a little lower than the Hα fibrils. The dominance of the blue wing contrast over the red wing contrast is much stronger in the Ca II line shown in the right panel, which indicates that the mean absorption profile of the Ca II fibrils is more blueshifted than that of the Hα fibrils, or blueshifted Ca II fibrils are more numerous than redshifted Ca II fibrils. Thus, supposing Hα fibrils and Ca II fibrils are not physically distinct, we conjecture that many Ca II fibrils may be identified with blueshifted Hα fibrils.

The most conspicuous features in the Ca II contrast profile plots are of course bright points. Even though the core intensity is still a minimum in most of the Ca II line profiles of the quiet region, these appear as emission features in that they are brighter than the average quiet Sun. The positive contrast is as high as 0.4 at the line center, and persists even in the wings. These bright points seen in the wings are the same as the photospheric magnetic points which appear brighter than the average quiet Sun in the continuum, G-band, UV, and broad-band Ca II H and K lines (see, *e.g.* Reardon, Uitenbroek, and Cauzzi, 2009).

4. Bisectors of Mean Spectral Profiles

4.1. The Quiet Region as a Whole

Figure 5 confirms that the bisector of the average Ca II line profile of the quiet region has an inverse C-shape. The peak of redshift of 5.1 pm – corresponding to 1.8 km s^{-1} – occurs at $I_1 = 0.27 I_c$ and $\Delta\lambda = 18$ pm, supporting the finding of Uitenbroek (2006) not only qualitatively, but also quantitatively in that the peak redshift we obtained is very close to 1.6 km s^{-1} reported by Uitenbroek (2006). Note that this average profile came from about 2.1×10^6 spectral profiles taken from both the network region and the IN, excluding some edges, and over half an hour. The observed redshift implies average downward motion in

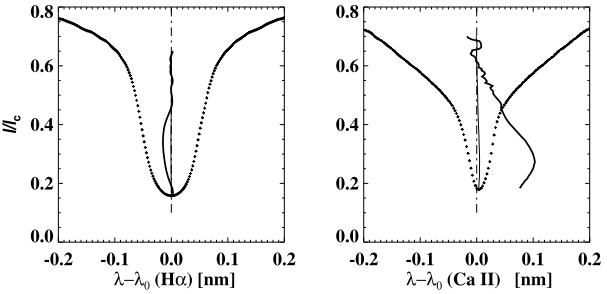

Figure 5 Enlarged presentations of the Hα line (left) and Ca II (right) profiles with the bisectors overplotted in dot-dashed curves. Thick curves represent the enhanced view of the bisectors with the wavelength offsets being magnified by a factor of 20.

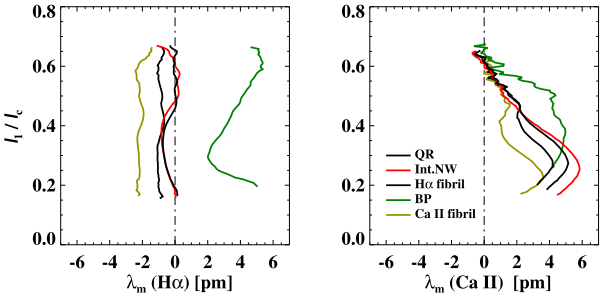

Figure 6 Plots of $I_1(\lambda_m)$ (bisectors) for each kind of features in the Hα line (left), and the Ca II line (right), respectively.

the rest frame of the solar center. We find that the upper portion of the bisector with higher values of intensity is close to the vertical line of zero Doppler shift, which is consistent with our expectation that the lower level of the atmosphere may be at rest at least in the average sense.

The bisector of the Hα line has a shape much different from that of the Ca II line. It is not of an inverse C-shape. Rather, it is almost vertically straight or, if not, of a weakly pronounced C-shape. The peak of blueshift occurs at $I_1 = 0.37 I_c$ and $\Delta\lambda = 47$ pm, and has a value of -1.0 pm – corresponding to 0.45 km s^{-1}. Interestingly, both the top and the bottom portions of the bisector are close to the vertical line of zero Doppler shift.

Our result on the bisector of the Hα line is apparently contrasted with Uitenbroek (2006) who made a brief remark that "the hydrogen Balmer α line bisector shows a hint of the pattern, with an amplitude of only 0.5 pm, corresponding to a downward motion of 228 m s^{-1}". However, this amplitude is so small that this remark might be rather interpreted as the indication that the shape of the bisector is close to a vertical line of zero shift, as our result does. The slight difference between our result and Uitenbroek (2006) might be due to the fact that the field of view in our observations is much smaller than that of Uitenbroek (2006) so that the areal fractions occupied by Hα fibrils and bright points, respectively, differ between the two studies.

4.2. Individual Features

Figure 6 presents the conventional bisectors – the plots of I_1 *vs.* λ_m – of the two lines for different kinds of features, and Figure 7 shows the plots of v_m *vs.* $\Delta\lambda$. This latter plot provides another way of displaying the spectral information contained in the bisectors. Roughly speaking, v_m for a smaller $\Delta\lambda$ reflects the line-of-sight velocity of the outer layer affecting the line, and v_m for a larger $\Delta\lambda$, that of the inner layer so that $v_m(\Delta\lambda)$ measures the variation of line-of-sight velocity over height. Note that for the construction of the average line pro-

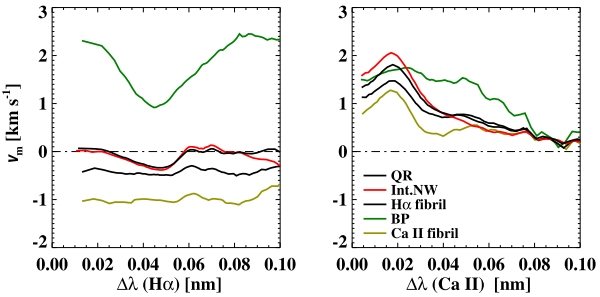

Figure 7 Plots of $v_m(\Delta\lambda)$ for each kind of features in the Hα line (left), and the Ca II line (right), respectively.

files in these figures, we used data from 30 raster scans obtained for 9 minutes, with the total numbers of spectral profiles being about 1.2×10^5 (30 % of the examined network area) for Hα fibrils, 3.5×10^4 (9 %) for Ca II fibrils, and 1.5×10^4 (4 %) for the Ca II bright points. Meanwhile the examined internetwork area contains about 2.5×10^5 pixels, 0.63 times the network area.

Figures 6 and 7 show that IN is similar to the whole quiet region in the shapes of the Hα line bisector and the Ca II line bisector. This similarity may be attributed to the fact that IN occupies a significant fraction of the quiet region, and it does not contain conspicuous inhomogeneous features such as fibrils and network bright points. This similarity also suggests that the observed characteristics of the bisectors of the quiet region as a whole described above may mostly originate from the structure and dynamics of IN. Not surprisingly, IN is truly representative of the quiet Sun. Since IN is characterized by the absence of noticeable magnetic structures and the presence of three-minute oscillations and acoustic shocks, it appears that the property of the bisectors such as the inverse C-shape of the Ca II line is more related to the oscillations and shocks than to the magnetic geometry.

The fibrils in the network region are different from IN in the shapes of the bisectors in several aspects. First, in comparison with IN, Hα fibrils are blueshifted by about 0.3 km s^{-1} in the Hα bisector and by 0.6 km s^{-1} in the Ca II bisector, and Ca II fibrils are blueshifted by about 0.6 km s^{-1} in the Hα bisector and by 0.7 km s^{-1} in the Ca II line bisector. Second, the Hα bisectors of the fibrils have shapes different from IN, being more straight. Third, the Ca II bisector of the Ca II fibrils contains a locally straight part as well as a part of inverse C-shape, so that its shape is not so regular as that of IN. The shape of the Ca II bisector of the Hα fibrils is a hybrid between the Ca II fibrils and IN. The difference between the Hα bisectors and the Ca II bisectors of the fibrils may be simply because at places where the fibrils are visible in Hα, the Ca II line still sees the underlying chromosphere that has basically the same property as the one in IN. The fibrils do not drastically alter the Ca II line profile of the light incident from below except for the noticeable reduction in the redshift.

The network bright points are much different from other features in the shapes of the bisectors. In the Hα line, the bisector is redshifted from the reference vertical line as much as 5.5 pm or 2.5 km s^{-1}, whereas the other bisectors either remain close to the reference line or are slightly blueshifted from it (see the left panels of Figures 6 and 7). The minimum redshift of about 2 pm occurs at $I_1 = 0.29 I_c$ and $\Delta\lambda = 47$ pm, which leads to a pronounced C-shape of the bisector. The shape of the Ca II bisector also is much different from others; neither it has a sharp redshift peak, nor the intensity of redshift peak coincides with others (see the right panels of Figures 6 and 7). Note that the large redshift of around 4 pm or 1.4 km s^{-1} persists at intensity values as high as $0.5 I_c$, indicating that not only the core, but also the wings are redshifted. The redshift in the bright points thus seems to originate from a wide range of the atmospheric levels.

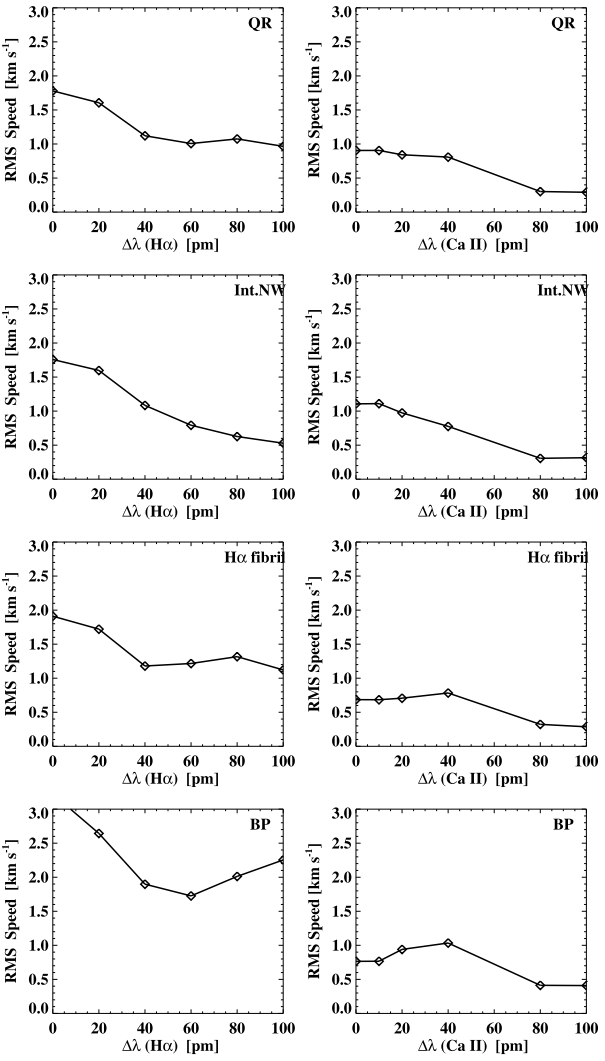

Figure 8 RMS fluctuations of v_m of the Hα line and Ca II 854.2 nm line, respectively, as functions of $\Delta\lambda$ for the quiet region as a whole, IN, the fibrils, and the bright points from top to bottom.

5. Spatio-Temporal Fluctuations of Doppler Shifts

Figure 8 presents the RMS Doppler shift fluctuations in the quiet region as a whole, and in each kind of identified features as functions of $\Delta\lambda$. We find that the Doppler shift fluctuation is the biggest at the line center ($\Delta\lambda = 0$) and decreases with $\Delta\lambda$, except for the bright points. This pattern in the Ca II line was previously noted by Evans and Michard (1962). It is the strongest in IN, being consistent with the picture of a stratified medium where the amplitude of velocity fluctuation increases with height to compensate for density drop.

Our measurements of Doppler shift fluctuations particularly at the line center and in the quiet region can be compared with previous measurements. We find that the RMS value is 1.8 km s^{-1} at the center of the Hα line. This value is bigger than 0.95 km s^{-1} in Table 2 of Evans and Michard (1962), but is smaller than 2.3 km s^{-1} reported by Cram, Brown, and

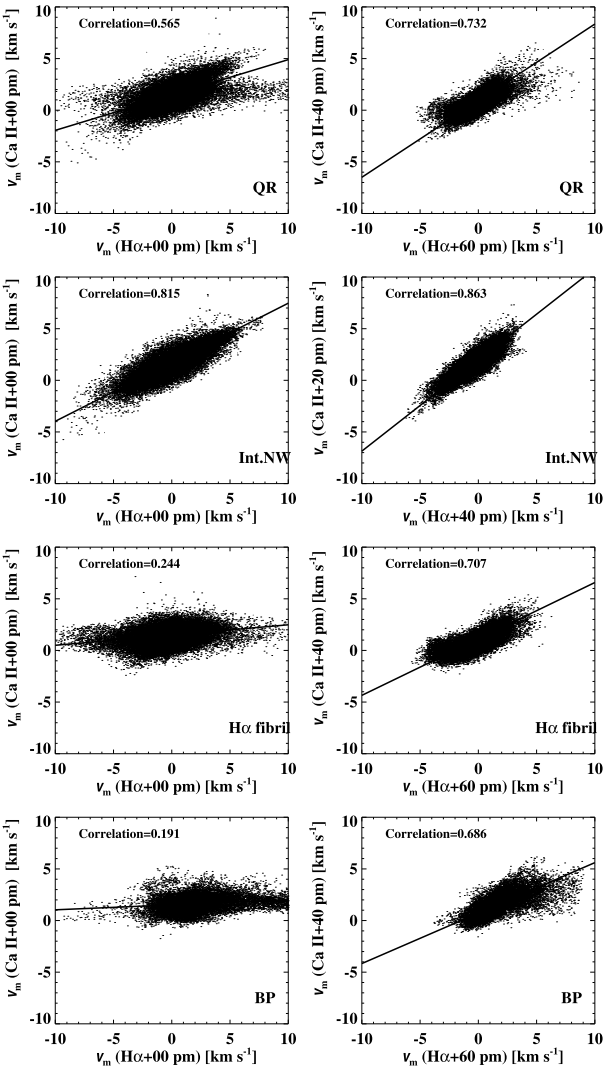

Figure 9 Scatter plots of the Hα v_m *vs.* from the Ca II v_m determined from the centers of the lines (left column) and those determined from the pair of $\Delta\lambda$ of the maximum cross-correlation (right column), for the quiet region as a whole, IN, the fibrils, and the bright points from top to bottom.

Beckers (1977). The RMS value we obtained at the Ca II 854.2 nm line center is 0.9 km s^{-1}, which is close to 0.87 km s^{-1} given in Table 3 of Evans and Michard (1962) and is smaller than 1.6 km s^{-1} reported by Cram, Brown, and Beckers (1977) and 1.4 – 1.5 km s^{-1} reported by Cauzzi *et al.* (2008). These discrepancies might be attributed either to the intrinsic region-to-region dependence of dynamical property or to the difference in the quality of seeing, as noted by Cram, Brown, and Beckers (1977).

Figure 9 presents the scatter plots showing the correlation between the two lines. We first compare between the cores of the lines and then between the two values of $\Delta\lambda$ displaying the maximum correlation. We are interested in these values because using them we can easily identify the same moving features in the two lines. They also serve as the observational basis for the understanding of how the two lines respond to the same moving features. In the quiet region as a whole, the correlation between the cores is moderate (0.57). This

value is very close to 0.58, the correlation coefficient of Ca II Doppler shift and Hα Doppler shift obtained by Cauzzi *et al.* (2009), and is a little smaller than 0.63, the value obtained by Cram, Brown, and Beckers (1977). The maximum correlation of 0.73 occurs between $\Delta\lambda = 60$ pm and $\Delta\lambda = 40$ pm. In IN, the correlation between the cores is fairly high, being 0.82, and the strongest correlation of 0.86 occurs between 40 pm and 20 pm. For the Hα fibrils, the correlation is weak between the cores, and has a peak of 0.71 between 60 pm and 40 pm. For the bright points, the correlation is even weaker, having a values of 0.19 between the cores, and a peak of 0.69 between 60 pm and 40 pm.

These observed correlations of Doppler shift between the Hα and Ca II lines may be understood based on our current knowledge of the formation of these lines in the solar chromosphere. Through the cores of these lines, we see the outer layer of the chromosphere. The strong correlation between the cores in IN supports that they sense about the same outer layer of the chromosphere in IN (Cauzzi *et al.*, 2009). The weak correlation in the fibrils originate from the fact that the Hα core is much more opaque than the Ca II core and hence senses fibrils while the Ca II core does not. The weak correlation in the bright points is mainly due to the contamination of the Hα spectral data by the fibrils. When all features are considered, the core velocities plot of the quiet region as a whole clearly shows different populations. Through the wings of the lines, we see the lower atmospheric layers where fibrils are not so important. This invisibility of fibrils strengthens the correlation between the wings of the two lines even in the region of fibrils, which naturally explains the strengthening of the correlation in the quiet region as well.

The observed RMS speeds and correlations of the Doppler shift in the bright points should be interpreted with caution for a couple of reasons. The first concern is the probable inadequacy of the lambdameter method in the Ca II core in the case it appears in emission, not in absorption. Our real investigation, however, shows that there is no indication of the emission core at least in the Ca II line data taken from the network region of our interest. The other and more realistic concern is the contamination of the spectral data by the fibrils that either overlie or neighbor the bright points. This contamination may be in charge of the large RMS speed of the Hα line (Figure 8) in bright points, as well as the poor correlation of the core velocities between the two lines (Figure 9). Thus we have to admit that our data and our analysis are not much suited for the study of the Doppler shift fluctuations in the bright points. In order to extract the pure spectral information of bright points, we will need high spatial resolution data, more careful identification preventing the contamination, and a bigger sample.

Figure 10 illustrates that the major origin of Doppler shift fluctuation in IN is three-minute oscillation. Shown in the figure are the analysis of the time series of the velocities taken from a single pixel inside IN. The power spectra are peaked at discrete frequencies of 4.1, 5.2, and 7.5 mHz. The maximum power frequency is 5.2 mHz, corresponding to the period of 190 s. This result is very consistent with previous studies (Lites, Rutten, and Kalkofen, 1993; Vecchio *et al.*, 2007; Rutten, van Veelen, and Sütterlin, 2008; Vecchio, Cauzzi, and Reardon, 2009; Cauzzi *et al.*, 2009; Kontogiannis *et al.*, 2010). Our new finding about three-minute oscillations in IN is that the variation of the Hα line Doppler shift and that of the Ca II line Doppler shift are almost in phase, irrespective of whether the pair of the cores or that of the inner wings is used. We estimate the time lag between the two lines at, if any, only a few seconds, with the Hα line Doppler shift variation slightly lagging behind the Ca II line Doppler shift variation.

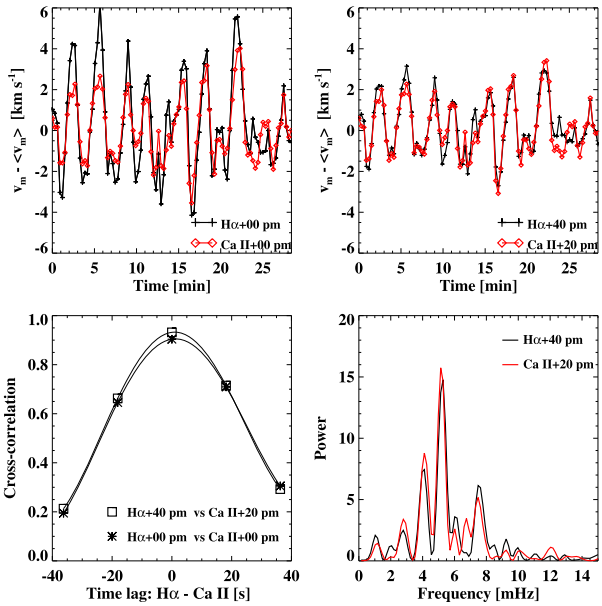

Figure 10 Top rows: temporal variations of Doppler shifts of the two lines determined at a single fixed point inside IN with different values of $\Delta\lambda$. Bottom left: the cross-correlation between the time series of Hα line Doppler shift and that of Ca II line Doppler shift. Bottom right: their power spectra.

6. Discussion

Internetwork regions are truly representative of the quiet Sun, so we first focus on the results obtained from IN inside the field of view of our observation. It is clear from our results that three-minute oscillations dominate this part and hence significantly affect the cores of these lines, and are responsible for the observed strong correlation of the Doppler shifts between the two lines, as was also remarked in previous observations (*e.g.* Rutten, van Veelen, and Sütterlin, 2008; Vecchio, Cauzzi, and Reardon, 2009). In this regard, the Hα line and the Ca II line appear to be very useful tools for the investigation of three-minute oscillations in the quiet Sun. The monotonic decrease of the RMS value with $\Delta\lambda$ in each line is quite consistent with the picture of a stratified medium with amplitude of velocity fluctuation exponentially increasing with height. The strong correlation and an insignificant phase difference between the two lines suggest that the formation heights of these lines are quite close to each other or different heights of the chromosphere oscillate in phase. Since the RMS values of the Ca II Doppler shifts are a little smaller than those of the Hα line, the average formation height of the Ca II line is likely to be a little lower than the Hα. From Figure 8, we estimate the RMS ratio of the Ca II line to the Hα line at $[0.6, 0.9]$. Supposing that these ratios are equal to $\exp(\Delta z/2H_{\rm p})$ where Δz is the difference in the formation height between the two lines, and $H_{\rm p}$ is pressure scale height, we obtain $\Delta z = [0.2, 1.0]H_{\rm p} \approx [40, 200]$ km.

Since the Hα line and the Ca II line do not differ much in the formation height, the observed contrast between these lines in the bisector shape of the mean profiles may be attributed to the different responses to the structure and dynamics of the outer chromosphere. The Ca II lines are much affected by collisional processes, and hence reflect the temperature of the line formation region. In contrast, the Hα line is dominated by radiative processes such as radiative excitation/deexcitation and photoionization/radiative recombination, and hence is insensitive to the local kinetic temperature in the chromosphere (*e.g.* Cauzzi *et al.*, 2009). The redshifted Ca II line bisector of an inverse C-shape suggests that for some reason, the Ca II line selects a little more of downflows than upflows while the Hα line does not.

The formation of the Ca II 854.2 nm line was studied by Uitenbroek (2006) with the non-LTE radiative transfer computations based on a snapshot from a simulation of solar convection (Asplund *et al.*, 2000). Leenaarts *et al.* (2009) computed synthetic Ca II 854.2 nm images by applying a three-dimensional non-LTE radiative transfer code to a radiation-MHD simulation of the solar atmosphere. These computations successfully reproduced various features seen in the blue wing and in the core, respectively. But they were not successful in reproducing the inverse C-shape of the observations. The spatially average profile computed by Uitenbroek (2006) was redshifted up to 0.5 $\mathrm{km\,s^{-1}}$ with respect to the central wavelength, but not so much as observed. In addition, both simulations (Uitenbroek, 2006; Leenaarts *et al.*, 2009) failed to produce the observed profiles especially near the cores; the simulated cores were much narrower and deeper than the observed ones. Leenaarts *et al.* (2009) attributed this discrepancy to the existence of motion in small scales of 0.1 Mm that future simulations with higher spatial resolution can resolve. The understanding of the Hα core formation in the chromosphere is more difficult because this line is strongly scattering and is much subject to non-local effects. Leenaarts, Carlsson, and Rouppe van der Voort (2012) confirmed that these non-local or smoothing effects are crucial for explaining the features observed through the core of this line; their 3D computation successfully reproduced predominantly dark, fibril-like features while their 1D computations failed to do that, only showing a distinctly photospheric scene.

Our results indicate that the simultaneous recording of the Hα line and the Ca II 854.2 nm line is a very useful diagnostic tool for the investigation of three-minute oscillations in IN. Note that the proper use of this tool, however, requires a correct knowledge on how these features affect the observed profiles of these lines. For example, Doppler velocities inferred from the line profiles using the lambdameter method may differ much from the true plasma velocities in the upper chromosphere, even though the two kinds of velocities are expected to be strongly correlated with each other. It should be kept in mind that the line is formed by the lower parts of the atmosphere as well. Therefore, the Doppler shift of the line should not be identified with the line-of-sight velocity of the outer part, but with a weighted average of the whole atmosphere. Generally speaking, since the lower parts of the atmosphere are likely to have lower line-of-sight velocities than the outer part, the velocity of the outer part may be higher than the inferred Doppler shift.

We plan to develop a simple model of radiative transfer in order to extract the Doppler velocity, Doppler width and other parameters of the outer part only from the observed line profile. A well-known model that has been widely used for a similar purpose was the cloud model developed by Beckers (1964). This cloud model can be successfully applied to light-scattering features lying high above other chromospheric features, but not to features embedded in the chromosphere such as waves and shocks. With a new cloud model applicable to the embedded features being available, we will be able to determine the Doppler widths in waves and shocks in IN and hence will be able to infer their temperatures. Note that this simple model is for the inversion only and is not like, for example, the forward physical model of Leenaarts, Carlsson, and Rouppe van der Voort (2012) that reproduces fibril-like structures by combining radiation-MHD simulations and full non-LTE radiative transfer computations. We also plan to improve the imaging quality of the FISS observations based on the upgrade of the AO and the relay optics. With these two things done, we will able to fully exploit the capability of the simultaneous recording of the Hα line and Ca II 854.2 nm line to reveal the origin of asymmetries in these lines as well as for the study of three-minute oscillations in IN and other features in network regions.

Acknowledgements We are grateful to the referee for a number of constructive comments. This work was supported by the National Research Foundation of Korea (2011-0028102) and by the Development of Korean Space Weather Center, a project of KASI.

References

Asplund, M., Nordlund, Å., Trampedach, R., Allende Prieto, C., Stein, R.F.: 2000, *Astron. Astrophys.* **359**, 729.

Beckers, J.M.: 1964, A Study of the Fine Structures in the Solar Chromosphere. Ph.D. Thesis, University of Utrecht.

Cauzzi, G., Reardon, K.P., Uitenbroek, H., Cavallini, F., Falchi, A., Falciani, R., Janssen, K., Rimmele, T., Vecchio, A., Wöger, F.: 2008, *Astron. Astrophys.* **480**, 515.

Cauzzi, G., Reardon, K., Rutten, R.J., Tritschler, A., Uitenbroek, H.: 2009, *Astron. Astrophys.* **503**, 577.

Chae, J., Park, H.-M., Ahn, K., Yang, H., Park, Y.-D., Nah, J., Jang, B., Cho, K.-S., Cao, W., Goode, P.R.: 2012, *Solar Phys.* doi:10.1007/s11207-012-0147-x.

Cram, L.E., Brown, D.R., Beckers, J.M.: 1977, *Astron. Astrophys.* **57**, 211.

Deubner, F.-L.: 1974, *Solar Phys.* **39**, 31.

Deubner, F.-L., Fleck, B.: 1990, *Astron. Astrophys.* **228**, 506.

Deubner, F.-L., Waldschik, T., Steffens, S.: 1996, *Astron. Astrophys.* **307**, 936.

Evans, J.W., Michard, R.: 1962, *Astrophys. J.* **135**, 812.

Gray, D.F.: 1992, *The Observation and Analysis of Stellar Photospheres*, Cambridge University Press, Cambridge, 417.

Kontogiannis, I., Tsiropoula, G., Tziotziou, K., Georgoulis, M.K.: 2010, *Astron. Astrophys.* **524**, A12.

Leenaarts, J., Carlsson, M., Rouppe van der Voort, L.: 2012, *Astrophys. J.* **749**, 136.

Leenaarts, J., Rutten, R.J., Sütterlin, P., Carlsson, M., Uitenbroek, H.: 2006a, *Astron. Astrophys.* **449**, 1209.

Leenaarts, J., Rutten, R.J., Carlsson, M., Uitenbroek, H.: 2006b, *Astron. Astrophys.* **452**, L15.

Leenaarts, J., Carlsson, M., Hansteen, V., Rouppe van der Voort, L.: 2009, *Astrophys. J. Lett.* **694**, L128.

Leighton, R.B., Noyes, R.W., Simon, G.W.: 1962, *Astrophys. J.* **135**, 474.

Lites, B.W., Rutten, R.J., Kalkofen, W.: 1993, *Astrophys. J.* **414**, 345.

Mein, N., Mein, P.: 1976, *Solar Phys.* **49**, 231.

Reardon, K.P., Uitenbroek, H., Cauzzi, G.: 2009, *Astron. Astrophys.* **500**, 1239.

Rouppe van der Voort, L., Leenaarts, J., de Pontieu, B., Carlsson, M., Vissers, G.: 2009, *Astrophys. J.* **705**, 272.

Rutten, R.J.: 2010, *Mem. Soc. Astron. Ital.* **81**, 565.

Rutten, R.J., van Veelen, B., Sütterlin, P.: 2008, *Solar Phys.* **251**, 533.

Sekse, D.H., Rouppe van der Voort, L., De Pontieu, B.: 2012, *Astrophys. J.* **752**, 108.

Scoas-Navarro, H., Elmore, D.: 2005, *Astrophys. J. Lett.* **619**, L195.

Uitenbroek, H.: 2006, *Astrophys. J.* **639**, 516.

Vecchio, A., Cauzzi, G., Reardon, K.P.: 2009, *Astron. Astrophys.* **494**, 269.

Vecchio, A., Cauzzi, G., Reardon, K.P., Janssen, K., Rimmele, T.: 2007, *Astron. Astrophys.* **461**, 1.